INSTITUTE OF PHYSICS PUBLISHING JOURNAL OF PHYSICS D: APPLIED PHYSICS

J. Phys. D: Appl. Phys. **40** (2007) 401–408 doi:10.1088/0022-3727/40/2/017

On the plasma rotation in a straight magnetized filter of a pulsed vacuum arc

L Giuliani[1], **D Grondona**[2], **H Kelly**[2] **and F O Minotti**[2]

Instituto de Física del Plasma (CONICET)—Departamento de Física, Facultad de Ciencias Exactas y Naturales, Universidad de Buenos Aires, Ciudad Universitaria Pab. I, 1428, Buenos Aires, Argentina

Received 26 September 2006, in final form 9 November 2006
Published 5 January 2007
Online at stacks.iop.org/JPhysD/40/401

Abstract

In vacuum arcs of interest for ion deposition, in which a magnetic filter is used, significant plasma rotation about the filter axis can develop. In the present work we present experimental evidence and simplified models to interpret relatively fast rotation of plasma generated in a pulsed vacuum arc with a straight magnetic filter and with a magnetic field strength in the range 52–430 G. The plasma rotation is produced in the first part of the filter (the driving region) where either the expanding or the contracting plasma encounters a mainly axial magnetic field. In the next part of the filter (the rotation region) a quasi-equilibrium is achieved and the plasma does not evolve further significantly. A rigid-rotor type of equilibrium is considered to model the rotation region, with experimentally obtained parameters, and a simple model is employed in the driving region to quantify the magnitude of the plasma rotation. It is found that at the quoted values of the magnetic field plasma rotation is an essential constituent to consider in any self-consistent theoretical model for the plasma inside the filter.

1. Introduction

Cathodic vacuum arcs are intense sources of metallic ions, which are often used to produce coatings [1]. The ions, coming from minute sites on the cathode surface ('spots'), are ejected with a broad range of kinetic energies (15–120 eV, depending on the cathode material and the charge-state of the ions [2–4]), and with a total ion current (I_i) proportional to the total discharge current (I_d). Under vacuum operating conditions, it has been found that $I_i/I_d \approx 0.08$–0.1 [5].

Cathodic arcs also produce micro-droplets of the cathode material that for some applications deteriorate the coatings. A widely employed method for removing these micro-droplets is magnetic filtering [6–8]. The filter consists of a duct (∼10–40 cm long) with an axial magnetic field of strength in the range of 50–650 G that confines the electrons but usually not the ions. The plasma is guided through the duct by the magnetic field, while the massive micro-droplets hit and eventually stick to the walls of the duct. The simplest arrangement used to guide the plasma is an annular anode followed by a straight duct with an externally applied axial magnetic field [9–14].

A very similar device to the vacuum arc with a straight magnetic filter is the so-called vacuum arc centrifuge [15]. In this case, a larger duct (∼100 cm long) with a more intense axial magnetic field (intensity ∼1000–2000 G) is usually employed to separate metal isotopes by a centrifugal effect resulting from plasma rotation. It is clear that the question of determination and prediction of plasma rotation is an important topic with vacuum arc centrifuges.

On the other hand, when magnetic filters are employed in coating applications of vacuum arcs, a not originally intended plasma rotation arises, which in some cases can be very significant. The plasma rotation in these latter devices is usually considered only in reference to curved magnetic filters, for which the drift out of the filter axis of the plasma makes the rotation apparent and of importance for the applications. In the case of straight filters the effect of rotation is not so evident and is usually not considered in the theoretical models [16–18]. At high enough values of the magnetic field, plasma rotation is an important constituent to consider in any self-consistent theoretical model for the plasma, since it controls the radial profiles of the plasma quantities inside the filter.

Straight, axially symmetric rotating plasma equilibria of the rigid-rotor type are predicted theoretically [19] and,

[1] Fellow of CONICET
[2] Member of CONICET

with more or less approximation, verified in the experiments [15, 20]. In this kind of equilibrium the electrostatic plasma potential has a quadratic dependence on the distance to the symmetry axis, and the plasma density radial distribution is well approximated by a Gaussian centred on this axis. Roughly, two main regions can be identified, the one where the rotating plasma equilibrium is verified, the rotation region, and the other where the rotation is originated, the driving region.

In the case of a vacuum arc centrifuge the driving region is that between the cathode and the anode grid, where the plasma column expands in the presence of a magnetic field with components in the axial and radial directions. The rotation is driven by the Lorentz force on the radial and axial electric density current components, plus additional effects that may enhance or oppose this driving [21]. After the grid, in the rotation region, in which the magnetic field has a mainly axial component, the above mentioned equilibrium is verified, with little additional variation of rotational velocity [22].

For vacuum arcs of interest for ion deposition one has a low density plasma column of rapid ions and electrons leaving the main discharge that expands away from the cathode and enters the magnetic filter. The magnetic field is usually intense enough to produce significant rotation only inside the filter. One could thus consider a driving region inside the filter where either the expanding or the contracting plasma encounters a mainly axial magnetic field, and a rotation region where the equilibrium is achieved and the plasma does not evolve further.

From the point of view of coating applications, it is also interesting to address the amount of plasma rotation, to evaluate the relative magnitude of the ion velocity tangential component with respect to the normal ion velocity.

In the present work we present experimental evidence and simplified models to interpret relatively fast rotation of plasma generated in a pulsed vacuum arc with a straight magnetic filter. The rigid-rotor type of equilibrium is considered to model the rotation region, with experimentally obtained parameters. A simple model is also employed in the driving region to quantify the magnitude of the plasma rotation.

2. Experimental apparatus and procedure

The arc was produced by discharging an electrolytic capacitor bank with $C = 0.075\,\mathrm{F}$, connected to a series inductor–resistor ($L = 2\,\mathrm{mH}$, $R = 0.33\,\Omega$), which critically damped the discharge [14]. The charging voltage was 260 V. The vacuum chamber was a stainless steel cylinder 25 cm long with a 10 cm (inner) diameter. The chamber pressure was maintained at a base pressure $<10^{-2}$ Pa during the whole arc discharge with an oil diffusion pump. A grounded cathode (5 cm in length and 1 cm in diameter) was located in front of an annular anode with an aperture of 5 cm and a thickness of 2 cm. The distance between the cathode frontal surface and the closest plane of the anode was 1 cm. The lateral surface of the cathode was covered with a Pyrex insulator, in order to ensure that the ion emission was through the cathode front surface. A mechanically controlled tungsten trigger rod ignited the arc. At the end of the anode was placed the entrance of the magnetic duct. The magnetic field was established by an external coil wrapped around a stainless steel tube (22 cm long, 5 cm inner diameter). The coil was fed with dc current from an independent power source. The magnetic field strength was measured with a calibrated Hall probe, and the magnetic field intensity (B) was characterized with the value measured at the duct centre. The range of B values investigated was 52–430 G. The filter was also biased with another independent power source that could withstand bias currents of up to 50 A. By inserting a small resistor ($\approx 1\,\Omega$) in series with the filter biasing source, the current collected by the filter (I_f) was determined. In practice, since the plasma floating potential (V_pf) in our case was higher than 20 V (see section 3, below), the filter was biased at a nominal voltage of 80 V (with a resulting actual bias voltage, V_bf, depending on the current collected by the filter). Also, filter voltages of $V_\mathrm{bf} = 0$ (ground) and $V_\mathrm{bf} = V_\mathrm{ff}$ (floating) were investigated. To insulate the duct from the arc discharge (mainly at a high filter bias voltage) a thin glass tube 4 cm long and with an outer diameter practically coincident with the duct inner diameter was glued to the insulating piece that coupled the anode and the duct. In this way, the duct acted as an insulator for the first 4 cm of its length.

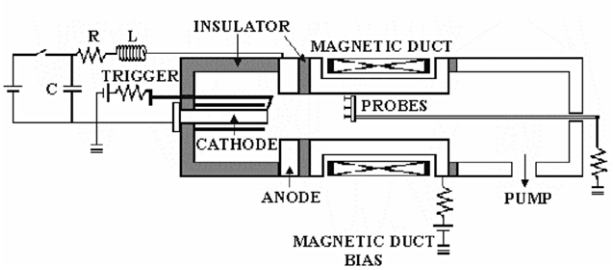

Figure 1. Schematic drawing of the experimental apparatus.

The chamber pressure was measured with a Pirani gauge with a range of up to 10^{-2} Pa. The arc voltage drop (V_ac) and the discharge current (I_d) were measured using a resistive high-impedance voltage divider and a calibrated small value resistor, respectively. Three circular plane copper probes (0.6 cm diameter) located at different radial positions in the tube were employed to register the plasma floating potential and the ion saturation current (I_i) as functions of the axial position along the tube (d), B and V_bf. One of the probes (probe 1) was located on the symmetry axis of the duct, while the other two (probes 2 and 3) were located at radial positions of 1 and 2 cm from the duct axis (measured from the centre of the coils), respectively. An additional large plane copper probe with a diameter of 4.5 cm (probe 4) was also employed to measure the total ion current flowing through the duct. Taking into account the relatively high plasma potential (see section 3, below), for the measurement of the ion saturation current the probes were simply biased to ground through a small resistance to ensure that the probe voltage was smaller than V_pf during the discharge. The electrical signals were registered using a four-channel digitizing oscilloscope (500 MS s^{-1} sampling rate, 100 MHz analogical bandwidth).

A schematic drawing of the experimental apparatus is shown in figure 1.

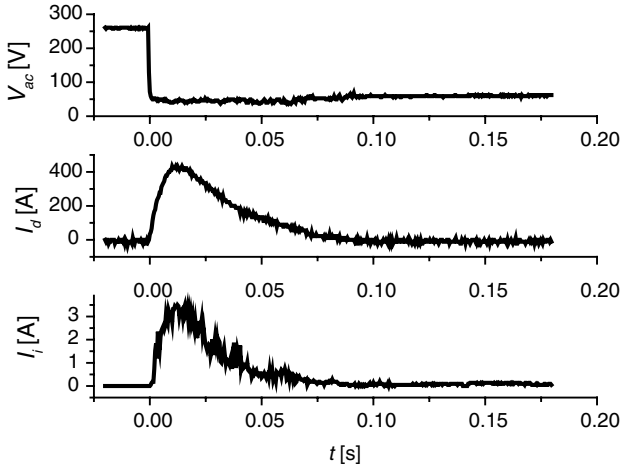

Figure 2. Typical waveforms of the arc voltage (top), total discharged current (centre) and ion current inside the filter (bottom).

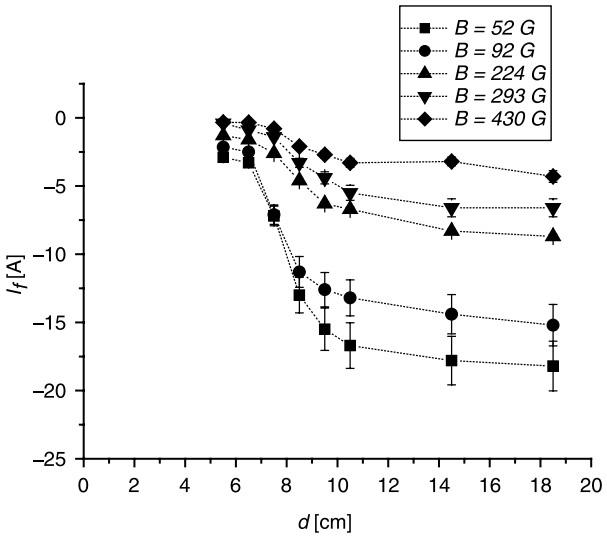

Figure 3. Axial distribution of the current collected by the filter. The lines are only a guide for the eye.

3. Results

Since vacuum arcs are known to present marked fluctuations, five consecutive shots were performed under the same operating conditions, so each point in the graphs to be presented below will correspond to the average of these shots. In figure 2, typical signals of V_{ac}, I_d, and I_i corresponding to $B = 224\,G$ are presented. The arc voltage drop (top of the figure) falls from the initial charging voltage value (260 V) during a closing time $\sim$1 ms, and then reaches an approximately constant value of 40 ± 5 V during the whole duration of the discharge. The discharge current waveform (centre of the figure) corresponds to a critically damped *RLC* series circuit, reaching a maximum of $\approx$440 A at $t \approx 10$ ms. It was found that the values of V_{ac} and I_d were almost independent of B for the investigated B values. The ion current waveform was similar to I_d, but varied in amplitude depending on the values of the parameters. In order to establish correlations between the different measured quantities, in what follows we will use the peak values of I_d and I_i as representative of these quantities, without any distinction in the symbols.

The filter floating potential as a function of B showed a typical behaviour usually found in several research works with magnetized filters, increasing monotonically with B, from $\approx$30 V for $B = 52$ G up to $\approx$60 V for $B = 430$ G in this case.

The large probe (placed at different axial positions d along the filter) was employed to measure the axial distribution of the current collected by the filter. In figure 3 I_f as a function of d (measured from the cathode frontal surface) for several B values and for a nominal filter bias voltage of 80 V is presented. It can be seen that the current increases smoothly at the beginning (at positions in the vicinities of the glass tube quoted above), then rises rapidly (for d in the range 7–10 cm), until for $d \geqslant 10$ cm I_f again reaches a smooth behaviour with a slow increase along the rest of the tube. It can also be seen that I_f increases strongly when B decreases. The case $B = 0$ was not investigated because of the high values of I_f.

In figure 4 the axial profiles of V_{pf} corresponding to the three radial positions (V_{pf}^1, V_{pf}^2 and V_{pf}^3, respectively) is presented, for the two extreme values of B (52 G and 430 G)

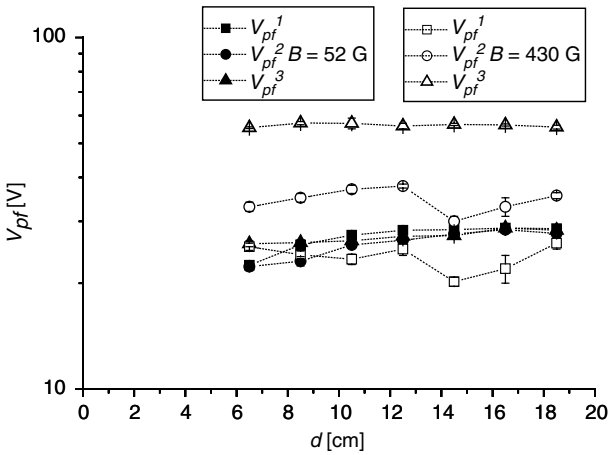

Figure 4. Axial profiles of the plasma floating potential corresponding to the three radial positions (V_{pf}^1, V_{pf}^2 and V_{pf}^3, respectively), for the two extreme values of B (52 G and 430 G) and for a nominal filter bias voltage of 80 V. The lines are only a guide for the eye.

and for a nominal filter bias voltage of 80 V. It can be seen that the profiles are practically independent of d, (a situation that was found for all the investigated B values) and that for the lower B values the profiles are practically coincident (within the experimental uncertainty), while for the higher B voltage differences of about 10–20 V appear between two consecutive probes, thus indicating the presence of a radial electric field (E_r). Intermediate B values corresponded also to intermediate profiles. Note that the floating voltages can be converted easily in plasma voltage (V_p) values, since in this problem elastic and inelastic collisions are infrequent (hence the electron temperature T_e can be considered as a constant), the magnetic field is almost perpendicular to the probe's surface [23] and classical Langmuir probe's theory corrected by Lam's work [24] to take into account ions of arbitrary kinetic energy is valid. Hence $V_p = V_{pf} + (T_e/e)\ \ln\{(2\pi m_i m_e)^{1/2} z^{-3/2}\ (1 + E_i/zT_e)^{-1/2}\}$, where T_e is the electron temperature in energy units, m_i and m_e are the ion and electron masses, respectively,

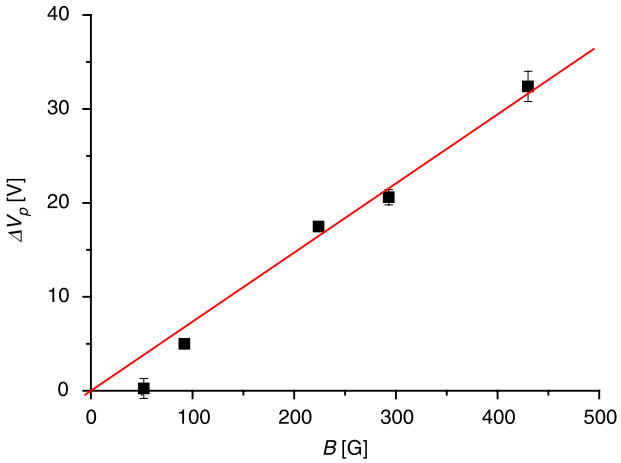

Figure 5. Difference $\Delta V_p = V_p^3 - V_p^1$ between the two extreme radial positions as a function of B for a generic axial position. The straight line represents the least square fit of the experimental points.

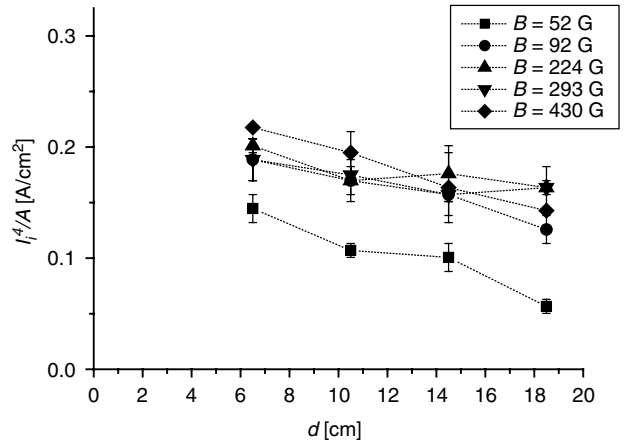

Figure 6. Total ion current (normalized to the probe area) flowing in the filter as a function of d. The lines are only a guide for the eye.

E_i is the ion kinetic energy and z the average charge of the ion. The electron temperature was determined from the slope of the electron current branch of the current–voltage characteristic of probe 1. To avoid misunderstandings in the interpretation of the electron branch of the probe characteristic due to the presence of the magnetic field, for the determination of T_e the case $B = 0$ and floating filter was selected, resulting in $T_e = 2.0 \pm 0.4$ eV.

In figure 5 the difference $\Delta V_p = V_p^3 - V_p^1$ between the two extreme radial positions as a function of B is presented (within experimental uncertainties, this difference was not sensitive to the d value). It can be seen that ΔV_p increases almost linearly with B.

The ion current to the probes decreased monotonically along the tube, and it was also found to be markedly dependent on B and also on V_{bf}. In figure 6 the ion current to the large probe I_i^4 as a function of d is presented, with B as a parameter, and in figures 7(a) and (b) examples of the ion current to the small probes (I_i^1, I_i^2 and I_i^3) as functions of d are presented, for $B = 430$ G and 52 G, respectively. The decrease in the total ion current shown in figure 6 gives the total ion losses to the filter. From figure 7 it can be seen that the current distribution along

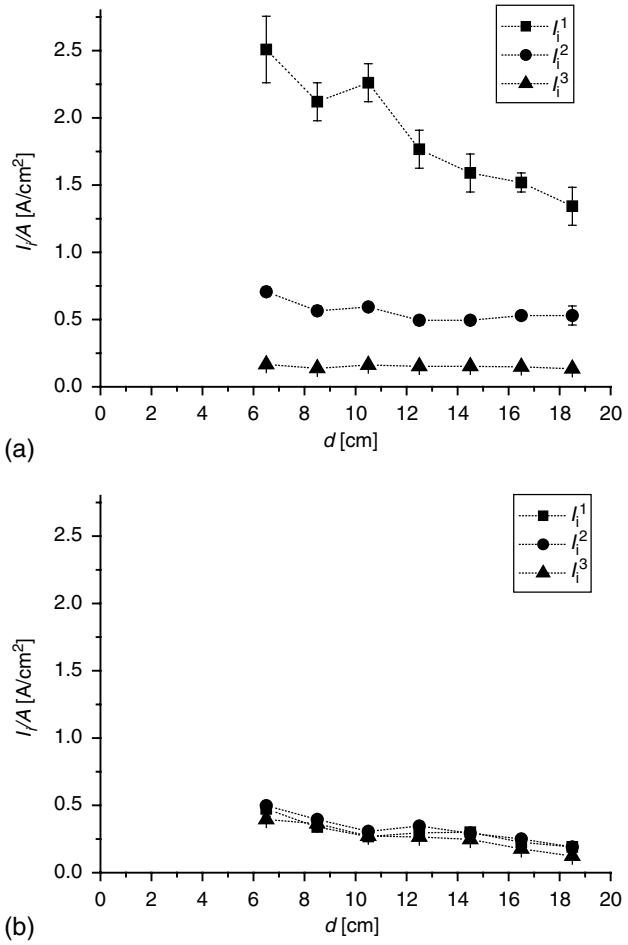

Figure 7. Ion current to the small probes (I_i^1, I_i^2, and I_i^3, normalized to the probe areas) set at different radial positions as functions of d for (a) $B = 430$ G; (b) $B = 52$ G. The lines are only a guide for the eye.

the tube results much more concentrated at the duct centre for large B values.

4. Interpretation of the results and discussion

From figure 3, one can note that almost all the electron current is collected by the filter in approximately the first five cm of the duct. The relatively small electron current collected by the filter at $d \geqslant 10$ cm is, however, high enough to mask the ion current that is also being collected (according to the decrease in the ion current profile shown in figure 6). Also note that the voltage radial distribution remains almost constant along the tube. The presented results thus suggest that there is a transition in the region located between the anode and some centimetre inside the duct entrance. After the transition region, the plasma quantities remain constant or vary very slowly along the duct (assuming that the plasma losses to the filter are relatively small), indicating that the plasma is in a quasi-steady state. This situation is especially noticeable for large B values (typically $B \geqslant 100$ G).

Let us investigate the fluid-like equations that rule the plasma structure within the quoted quasi-steady region. Neglecting the electron acceleration term (due to the smallness

of the electron mass), the electron momentum equation in the radial direction can be written as

$$T_e \frac{\partial}{\partial r} \ln n + eE_r + eB\Omega_e r = 0, \quad (1)$$

where n is the plasma density, and $\Omega_e r$ is the electron velocity in the azimuthal direction. Collisions between electron and ions have also been neglected in equation (1), since for the typical values of n and T_e found in this experiment, the collision term (ν_{ei} (u–u_e), where ν_{ei} is the electron–ion collision frequency and u and u_e are the ion and electron velocities, respectively) results more than one order of magnitude smaller than, for instance, the pressure gradient force. On the other hand, considering non-magnetized ions, the ion-momentum equation in the radial direction can be written as

$$m_i \left(u_r \frac{\partial u_r}{\partial r} + u_z \frac{\partial u_r}{\partial z} - \frac{u_\theta^2}{r} \right) = -\frac{T_i}{Z} \frac{\partial}{\partial r} \ln n + ZeE_r, \quad (2)$$

where Z for a copper cathode takes the value $Z \approx 2$ [25], T_i is the ion temperature ($T_i \approx 0.2$–0.3 eV, close to the boiling point of the cathode material [26]), and u_r, u_θ and u_z are the components in cylindrical coordinates of the ion velocity. It has been shown [17] that $u_r \sim r$, and $u_z \sim$ constant, so all the ion acceleration terms are proportional to the radial coordinate and the left-hand-side term in equation (2) can be written as - $m_i \Omega_i^2 r$. Note that Ω_i does not necessarily have the meaning of an angular velocity (this would be the case if the centripetal acceleration were the dominant term). Hence, the ion momentum equation can be written in an approximate form as

$$m_i \Omega_i^2 r - \frac{T_i}{Z} \frac{\partial}{\partial r} \ln n + ZeE_r = 0. \quad (3)$$

Equations (1) and (3) can be combined to eliminate n, and so the radial electric field can be expressed as

$$E_r = -\frac{\partial V}{\partial r} = -\left(1 + \frac{T_i}{Z^2 T_e}\right)^{-1} \frac{m_i}{Ze} \left(\Omega_i^2 + \frac{T_i}{Z^2 T_e} \omega_{ci} \Omega_e \right) r, \quad (4)$$

where $\omega_{ci} = ZeB/m_i$. Under the assumption that Ω_i and Ω_e are constants, (resembling the well known rigid-rotor solutions [19]), equation (4) can be immediately integrated to obtain the electrostatic potential

$$V(r) = V_0 + \frac{m_i}{2Ze} \left(\Omega_i^2 + \frac{T_i}{Z^2 T_e} \omega_{ci} \Omega_e \right) r^2, \quad (5)$$

where V_0 is the electrostatic potential value on the filter axis.

Replacing equation (4) into equations (1) or (3), the plasma density can be obtained as

$$n = n_0 \exp \left[\frac{m_i}{2ZT_e} (\Omega_i^2 - \omega_{ci} \Omega_e) r^2 \right], \quad (6)$$

where n_o is the plasma density at the filter axis.

A numerical inspection of equations (5) and (6) (using the experimental values of the parameters) shows that in order to fit the experimental data of plasma voltage and density it is required that $\Omega_i^2 \sim \omega_{ci}\ \Omega_e$ (this approximation will be better justified in what follows). Since $T_i/(Z^2 T_e) \ll 1$, one can neglect to the first order $(T_i/Z^2 T_e)\ \omega_{ci}\Omega_e$ as compared with Ω_i^2 in equation (5). Thus, employing the auxiliary variable $\delta^2 = -(\Omega_i^2 - \omega_{ci}\Omega_e)$ in equation (6), equations (5) and (6) are written as

$$V(r) \approx V_0 + \frac{m_i \omega_{ci} \Omega_e}{2Ze} r^2, \quad (7)$$

$$n = n_0 \exp \left(-\frac{m_i}{2ZT_e} \delta^2 r^2 \right). \quad (8)$$

Equation (7) is consistent with $V(r)$ being independent on the axial coordinate along the filter, which is precisely what is observed. Also, equation (7) predicts an increasing voltage radial profile from the filter axis and can be compared with the experimental data by noting that the voltage difference between two radial positions (i, j) can be written (after replacing the constants by their numerical values) in practical units as

$$\Delta V_{ij} = V_i - V_j(\mathrm{V}) = 4 \times 10^{-9} B(\mathrm{G}) \Omega_e [r_i^2 - r_j^2]\,(\mathrm{cm}^2). \quad (9)$$

Note that Ω_e (that represents a true electron rotating angular frequency) can be determined from the slope of ΔV_{ij} as a function of B for given values of r_i and r_j. This was done in figure 5, for $r_i = 2$ cm and $r_j = 0$ cm. The resulting value for the slope was 8.3×10^{-2} V G^{-1}, resulting in an Ω_e value of $(5.2 \pm 0.3)\ 10^6$ s^{-1}.

On the other hand, equation (8) serves to determine the δ^2 value from the ion current measurements. These ion measurements were converted to plasma density values by using non-collisional probe theory corrected with Lam's work [24] to take into account ions with arbitrary kinetic energy: $I_i = A \quad Zen\ \{2(ZT_e + E_i)/m_i\}^{1/2}$, where A is the probe area. In principle, δ^2 could be a function of the radial coordinate, but we have tried to adjust this parameter by assuming a Gaussian density radial profile, as usual theories predict [19]. This adjustment must be taken with caution, since there are only three radial experimental points (the location of more than three probes in the radial direction was not practical in this experiment due to the relatively small radius of the filter). As an example, in figure 8 we present a density profile adjusted with a Gaussian curve, for the case $B = 430$ G and $d = 6.5$ cm. From these profiles, the length scale (r_o) for the density decay can

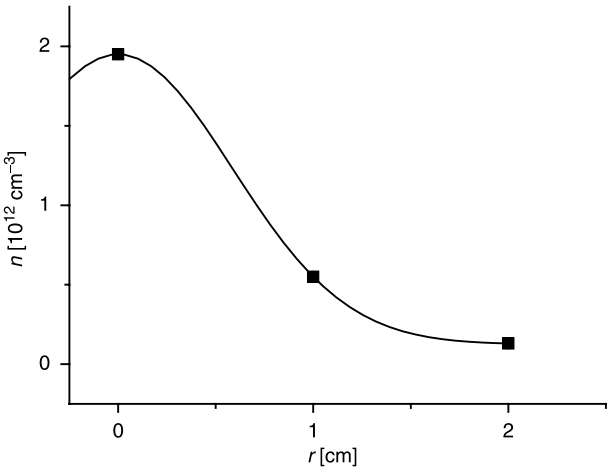

Figure 8. Radial plasma density profile adjusted with a Gaussian curve, for the case $B = 430$ G and $d = 6.5$ cm. The plasma density was obtained from the ion current measurements (see figure 7).

Table 1. Different parameters of the equilibrium model ($\omega_{ci}\Omega_e$, δ^2, r_o and Ω_i) obtained for each experimental B value. The last column presents the total rotation (Ω_T) obtained from the driving region model.

B (G)	$\omega_{ci}\Omega_e$ (10^{10} s^{-2})	δ^2 (10^{10} s^{-2})	r_o (cm)	Ω_i (10^5 s^{-1})	Ω_T (10^5 s^{-1})
430 ± 20	67 ± 7	17 ± 1	0.8 ± 0.1	8.2 ± 0.4	5.7
293 ± 15	46 ± 5	15 ± 1	0.9 ± 0.1	6.8 ± 0.3	3.0
224 ± 10	35 ± 4	14 ± 1	0.9 ± 0.1	5.9 ± 0.3	2.3
92 ± 5	14 ± 2	4.6 ± 1	1.6 ± 0.1	3.7 ± 0.2	0.2
52 ± 3	8 ±1	1 ± 1	3.5 ± 0.1	2.8 ± 0.2	

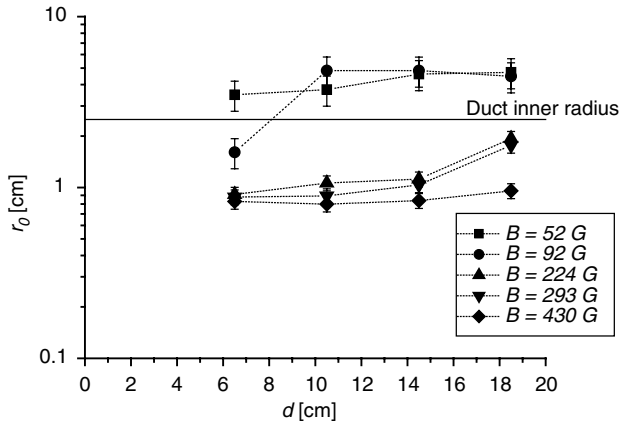

Figure 9. Spatial scale of radial density Gaussian decay as a function of d for several B values. The lines are only a guide for the eye.

be obtained, which is related to the δ value through the simple relationship (in practical units): r_o (cm) $= 3.5 \times 10^5/\delta(s^{-1})$.

In table 1 we present the obtained δ^2 values, the corresponding r_o values and the $\omega_{ci}\,\Omega_e$ values for all the values of the magnetic field and for $d = 6.5$ cm. The $\Omega_i = (\omega_{ci}\Omega_e)^{1/2}$ values are also included, and in the last column we have added a theoretical value (Ω_T) obtained from a simplified model for the driving region (see section 5). It can be seen from the table that the obtained values for δ^2 are well below the $\omega_{ci}\Omega_e$ values, thus sustaining the validity of the adopted approximation ($\Omega_i^2 \sim \omega_{ci}\Omega_e$). The derived values for Ω_i are in the range (2.8–8.2)$\times 10^5$ s^{-1}. As expected, the values of r_o decrease with an increasing magnetic field, indicating a more collimated plasma flux for high B values. The behaviour of the density profile along the tube is presented in figure 9, where r_o as a function of d, with B as a parameter, is plotted. As can be seen from figure 9, the larger the B value the more collimated is the plasma flux. For the largest value of B ($B = 430$ G) a quite collimated plasma flux (that is, $r_o \approx$ constant ~0.8 cm) is apparent, while the profile spreads along the filter for smaller B values (for $B < 100$ G the plasma completely fills the duct for $d > 10$ cm).

5. Driving region model

We now use a simple model to quantify the plasma rotation generated in the driving region. The model is similar to that used in [18] with the addition of plasma rotation around the symmetry axis of the discharge chamber of figure 1. We consider a stationary, axially symmetric plasma jet representing the ions and electrons leaving the main discharge and entering the filter. We concentrate on the fluid equations describing the ions, neglecting the collisions with electrons. Using the cylindrical coordinates already introduced, the charge conservation equation for the ion current density $\boldsymbol{j}$ is for the assumed symmetry,

$$\frac{1}{r}\frac{\partial}{\partial r}(rj_r) + \frac{\partial j_z}{\partial z} = 0. \tag{10}$$

As in [18] the axial current density j_z is assumed to be uniformly distributed in the cross section of the plasma jet, of radius $R(z)$. One thus obtains from equation (10)

$$j_z = \frac{I_i}{\pi R^2}, \qquad j_r = \frac{I_i R'}{\pi R^3} r, \tag{11}$$

where $R' \equiv \mathrm{d}R/\mathrm{d}z$ and I_i is positive as the positive z direction is that away from the cathode.

The ion mass density ρ and the axial ion velocity u_z are also considered uniform in each cross section of the jet. We are in this way modelling the core of a more realistic density distribution like, for instance, a Gaussian radial profile, assuming that practically all mass is included in this core; ρ and u_z are thus related by mass conservation as

$$\rho u_z \pi R^2 = G, \tag{12}$$

with G the (constant) ion mass rate of the jet. Thus the mass conservation equation

$$\frac{1}{r}\frac{\partial}{\partial r}(r\rho u_r) + \frac{\partial}{\partial z}(\rho u_z) = 0 \tag{13}$$

allows us to determine u_r as

$$u_r = \frac{GR'}{\rho\pi R^3} r. \tag{14}$$

The θ component of the ion-momentum conservation equation is (the viscous force is neglected and afterward verified to be small compared with the Lorentz force)

$$u_r\frac{\partial u_\theta}{\partial r} + u_z\frac{\partial u_\theta}{\partial z} + \frac{u_r u_\theta}{r} = -\frac{j_r B}{\rho}. \tag{15}$$

If in this equation the expressions for j_r, u_z and u_r from equations (11), (12) and (14) are used, and one expresses u_θ as $u_\theta = \Omega(z)r$, the following equation for $\Omega(z)$ is readily obtained:

$$\frac{\mathrm{d}\Omega}{\mathrm{d}z} + \frac{2R'}{R}\Omega = \frac{I_i B R'}{GR}. \tag{16}$$

The general solution of this equation is

$$\Omega = \frac{I_i B}{2G}\left[\left(\frac{R_{in}}{R}\right)^2 - 1\right], \tag{17}$$

where R_{in} is the jet radius at the entrance of the driving region, where $\Omega = 0$. In this way, the Lorentz force due to the radial current generates an ion rotation easily quantified by equation (17). At this point the viscous force (per unit volume) f_{visc} can be estimated as $f_{visc} = \eta_0(\nabla^2 u_\theta - u_\theta/r^2)$. Using the expression of η_0 given in [27], the form $u_\theta = \Omega(z)r$, and equations (11) and (14) for j_r and u_r, one can obtain for the ratio of f_{visc} to the Lorentz force $f_L = j_r B$ (the prime denotes a z derivative)

$$\frac{f_{visc}}{f_L} = \frac{\pi R^3 \eta_0 \Omega''}{I_i R' B}. \tag{18}$$

With the expression of $\Omega(z)$ obtained, and those of u_z and u_r in terms of $R(z)$, one easily obtains

$$\frac{f_{visc}}{f_L} = \frac{3\eta_0 u_r}{\rho R u_z^2}. \tag{19}$$

For the conditions of the experiment: $R \approx 1$ cm, $T_i \approx 0.3$ eV, $n_i \approx 5 \times 10^{11}$ cm^{-3}, and copper ions, the result is

$$\frac{f_{visc}}{f_L} = \frac{u_r}{u_z^2} 10^5 \text{ cm s}^{-1}. \tag{20}$$

As $u_z \approx 10^6$ cm s^{-1}, and u_r is at most a fraction of u_z, $f_{visc}/f_L \approx 0.1$ in the worst case. In this way the viscous force can be consistently neglected in the experiment considered.

As the ion current and the ion mass rate are proportional to each other, expression (17) for the total rotation Ω_T induced in the driving region reduces to

$$\Omega_T = \frac{ZeB}{2m_i}\left[\left(\frac{R_{in}}{R_{out}}\right)^2 - 1\right], \tag{21}$$

with R_{out} the radius of the jet leaving the driving region. In the configuration considered, we have a jet that contracts as it enters the filter and is guided by the magnetic field. A simple estimation for R_{in} is the inner filter radius, while R_{out} can be taken as the r_0 defined in the previous section. Using these estimations, the obtained values of Ω_T are shown in table 1. Reasonable values of Ω_T, comparable to those of Ω_i, are obtained for the three largest values of the magnetic field (for small B values practically no rotation is predicted). This gives the indication that the contribution of the centripetal acceleration to Ω_i in equation (3) is dominant in these cases and also gives support to the modelled driving mechanism.

It is worth noting that the ion tangential velocities obtained from the Ω_T values presented in table 1 correspond to ion rotational energies below 7 eV, which are almost one order of magnitude smaller than the average ion kinetic energy associated with the ion axial movement [25].

6. Final remarks

A somewhat detailed investigation of a metallic straight magnetic filter coupled to a pulsed vacuum arc has been presented. The floating plasma potential and ion saturation current as functions of the axial and radial coordinates in the filter have been obtained for several values of the axial magnetic field in the filter. Also, we have measured the electron temperature and the collected current distribution along the filter. It was found that almost all the current (electronic) is collected by the filter in approximately the first five cm of the duct. The plasma voltage, obtained from the floating voltage under the usual assumption of constant electron temperature, was almost independent of the filter axial coordinate, but presented a radial profile that increased linearly with the magnetic field strength. The plasma density (obtained from the ion saturation current) also presented a radial profile that spreads along the filter according to the magnetic field strength. The ion current in the plasma flux also showed a smooth decay along the filter. We have interpreted these results as supporting the presence of a plasma transition in the region located between the anode and some centimetres inside the duct entrance (the driving region). After the driving region, the plasma quantities remain constant or vary very slowly along the duct (assuming that the plasma losses to the filter are relatively small), indicating that the plasma is in a quasi-steady state with negligible variations in the axial direction. We have proposed that the electron and ion-momentum equations determine the plasma structure inside the filter. With some simple assumptions (neglecting electron-ion collisions, constant angular rotation velocities of electrons and ions in the azimuthal direction, constant electron and ion temperatures) it was possible to obtain the radial profiles of the electrostatic potential and plasma density. These profiles matched reasonably well the experimental profiles for appropriate values for the ion and electron angular frequencies. The electrons rotate with a constant angular velocity that is intermediate between the electron cyclotron frequency and the electron drift angular velocity, while the ions rotate in the same direction of the electrons with an angular velocity dependent on the magnetic field strength. The difference between these two velocities rules the radial scale length of the plasma density.

To summarize, the experimental evidence collected in this work indicates that the plasma is in a quasi- steady state in the filter for high values of the magnetic field (being the filter losses sufficiently small so as not to perturb this equilibrium), and that rotation of the plasma is an essential constituent to consider in any self-consistent theoretical model for the plasma inside the filter. Since the ion kinetic energy associated with the rotational motion is much smaller than that corresponding to the ion axial motion, remarkable effects on the coating structure are not expected. In any case, an impinging ion on the substrate surface with certain tangential velocity may be useful since this velocity component would improve the ion lateral mobility along the surface, thus contributing to a more homogeneous coating growth.

Acknowledgments

This work was supported by grants from the Buenos Aires University (X 111 and X 106), the CONICET (PIP 5378) and the ANPCyT (ID03-09491).

References

[1] Boxman R, Sanders D and Martin P 1995 *Handbook of Vacuum Arc Science and Technology, Fundamentals and Applications* (Park Ridge, NJ: Noyes)
[2] Plyutto A A, Ryzhkov V N and Kapin A T 1965 *Sov. Phys. —JETP* **20** 257–60

[3] Davis W D and Miller H C 1969 *J. Appl. Phys.* **40** 2212–21
[4] Lunev V M, Padalka V G and Khoroshikh V M 1977 *Sov. Phys.— Tech. Phys.* **22** 858–61
[5] Kimblin C W 1973 *J. Appl. Phys.* **44** 3074–81
[6] Aksenov I I, Belous V, Padalka V G and Khoroshikh V M 1979 *Sov. J. Plasma Phys.* **4** 425–8
[7] Anders S, Anders A and Brown I 1993 *J. Appl. Phys.* **74** 4239–41
[8] Boxman R L, Zhitomirsky V, Alterkop B, Gidalevich E, Keidar M and Goldsmith S 1996 *Surf. Coat. Technol.* **86–87** 243–53
[9] Cohen Y, Boxman R L and Goldsmith S 1989 *IEEE Trans. Plasma Sci.* **17** 713–16
[10] Storer J, Galvin J and Brown I 1989 *J. Appl. Phys.* **66** 5245–50
[11] Cluggish B 1998 *IEEE Trans. Plasma Sci.* **26** 1645–52
[12] Zhitomirsky V N, Zarchin O, Boxman R L and Goldsmith S 2002 *Proc. 20th Int. Symp. on Discharges and Electrical Insulation in Vacuum (Tours, France)* pp 670–3
[13] Zang T, Tang B, Zeng Z, Chen Q, Chu P and Brown I 1999 *IEEE Trans. Plasma Sci.* **27** 786–9
[14] Kelly H, Giuliani L and Rausch F 2003 *J. Phys. D: Appl. Phys.* **36** 1980–6
[15] Krishnan M, Geva M and Hirshfield J L 1981 *Phys. Rev. Lett.* **46** 36–9
[16] Keidar M, Beilis I and Brown I G 1998 *J. Appl. Phys.* **84** 5956–61
[17] Keidar M, Beilis I, Boxman R L and Goldsmith S 1996 *J. Phys. D: Appl. Phys.* **29** 1973–83
[18] Krinberg I A 2005 *IEEE Trans. Plasma Sci.* **33** 1548–52
[19] Davidson R C 1976 *Phys. Fluids* **19** 1189–202
[20] Del Bosco E, Simpson S W, Dallaqua R S and Montes A 1991 *J. Phys. D: Appl. Phys.* **24** 2008–13
[21] Simpson S W, Dallaqua R S and Del Bosco E 1996 *J. Phys. D: Appl. Phys* . **29** 1040–46
[22] Yue Y and Simpson S W 1996 *J. Phys. D: Appl. Phys.* **29** 2866–72
[23] Koch B, Bohmeyer W and Fussmann G 2003 *J. Nucl. Mater.* **313–316** 1114–18
[24] Lam S 1965 *Phys. Fluids* **8** 7383
[25] Anders A and Yushkov G 2002 *J. Appl. Phys.* **91** 4824–32
[26] Minotti F, Kelly H and Lepone A 2002 *Plasma Sources Sci. Technol.* **11** 294–301
[27] Braginskii S I 1965 *Reviews of Plasma Physics* vol 1, ed M A Leontovich (New York: Consultants Bureau) p 205